

DOI 10.24425/aee.2022.142111

Performance comparison of double stator permanent magnet machines

CHUKWUEMEKA CHIJOKE AWAH 

*Department of Electrical and Electronic Engineering
Michael Okpara University of Agriculture
Umudike, PMB 7267, Umuahia, Abia State, Nigeria
e-mail: awahchukwuemeka@gmail.com*

(Received: 26.02.2022, revised: 13.07.2022)

Abstract: The electromagnetic and output performance characteristics of three (3) different types of double stator permanent magnet machines are quantitatively compared and presented in this study, in order to determine the most promising machine topology amongst the considered machine types, for potential practical applications(s). Two-dimensional (2D) and three-dimensional (3D) finite element analysis (FEA) methods are deployed in the computation of the performance metrics using ANSYS-MAXWELL software. The compared machines in this work are designated as: Machine 1, Machine 2 and Machine 3, respectively. The investigated machines have varying structural arrangements and two separate excitation sources. Machine 1 has its magnets situated in the outer stator with corresponding armature windings on both inner and outer stators. The magnets of Machine 2 are located in its inner stator while it has armature windings on both inner and outer stator parts. More so, Machine 3 is equipped with magnets in its inner and outer stators, though without armature windings on the inner stator section. The considered performance metrics include: induced-electromotive force (induced-EMF), torque, power, demagnetization, losses and efficiency. The results show that the investigated Machine 3 has higher induced-EMF value and more sinusoidal electromotive force waveform than the other compared machines. Consequently, Machine 3 also has larger electromagnetic torque and power. Moreover, Machine 1 has the best flux-weakening potential, obtained from both the ratio of its maximum speed to base speed and the flux-weakening factor (k_p).

Key words: demagnetization, double stator, induced voltage, losses, power and torque



© 2022. The Author(s). This is an open-access article distributed under the terms of the Creative Commons Attribution-NonCommercial-NoDerivatives License (CC BY-NC-ND 4.0, <https://creativecommons.org/licenses/by-nc-nd/4.0/>), which permits use, distribution, and reproduction in any medium, provided that the Article is properly cited, the use is non-commercial, and no modifications or adaptations are made.

1. Introduction

Recently, investigations on double stator (DS) permanent magnet (PM) machines are on the increase, owing to its enviable performance(s) over the single stator machines; meanwhile, a lot of different dual stator PM machine topologies are still emerging, in order to improve on the already good electromagnetic and output performances of such family of machines. Hence, three different double stator permanent magnet machine types are developed and compared in this present study in order to predict, evaluate and compare their overall electromagnetic and output performances/characteristics.

Comprehensive account of assorted magnetically-g geared permanent magnet machines with either dual rotor or dual stator configurations is presented in [1]; however, it is noted that most of the reviewed magnetically-g geared machines have complicated structural architecture and that would likely lead to high manufacturing cost of the machines. It is worth noting that the compared machines in this current study would function as both a magnetically-g geared machine and a flux-switching permanent magnet machine, owing to its ability to modulate the generated magnetic fields of the PMs and armature coils in addition to its inherent capability to instantaneously change the produced flux path, in one-half electric cycle. Similarly, a comparative study of different double stator permanent magnet machines is presented in [2] with a view to identifying the machine topology with the most admirable electromagnetic output, for possible direct-drive implementation. It is proved that the machine types having a single tooth per stator pole has better performances, in terms of reduced voltage harmonics as well as minor torque ripples and better output torque than the ones with multi-tooth per stator pole geometric plan. It could be observed that the examined machines would have high heating effect owing to the location of the PMs on the rotatory part of the machine, coupled with large PM usage in a limited space, thereby creating chances of magnetic flux leakages in such a system relative to the architectural and working plan of the double stator PM machines in this current investigation. Moreover, the stator and rotor pole number combinations of a given electrical machine could ultimately affect the ensuing output performance. Thus, it is demonstrated in [3] that the output performance of a given electrical machine, ranging from its torque characteristics to efficiency, would largely depend upon the machine's winding configurations as well as the slot and pole number arrangements. Therefore, choice of feasible slot and rotor pole combinations should be taken seriously in the design process of electrical machines. It is worth noting that concentrated winding configuration in the above study would yield higher economic benefits due to its shortened winding coils; additionally, it has improved efficiency and reduced torque ripple characteristics relative to the results from the equivalent machine having distributed winding topology. By extension, the implemented concentrated winding arrangement in this current study would most likely be more efficient than its distributed winding counterparts. The great influence of winding topologies on output characteristics of electrical machines is reconfirmed in [4]. The adopted winding type in this current study is double layer non-overlapping winding configuration while having its optimum stator and rotor pole combinations, in order to achieve the most effective electromagnetic performance from the investigated machines.

A double stator permanent magnet (DSPM) machine suitable for wind energy generation applications is recommended in [5]. The recommended machine is furnished with toroidal armature windings in both stators and this particular winding arrangement is claimed to give the machine a

higher flexibility to operate under varying modes and at different rotor speed for improved overall machine efficiency, compared to other permanent magnet machines. More so, the influence of rotor and stator pole permutations on the overall performance of the machine is also demonstrated. However, the recommended DSPM machine would suffer from poorer thermal instability unlike the compared flux-switching double stator machine in this present investigation, due to the relative PM location on the rotational part of the DSPM machine with an expected heightened eddy current loss value. Similarly, a low speed high torque dual stator machine suitable for direct-drive applications is proposed and optimized in [6]. Again, the proposed dual stator machine has its permanent magnets (PMs) sandwiched in its rotor segments; thus worsening the machine's thermal management capability. Additionally, the ability of a permanent magnet machine to efficiently operate under different working conditions with increased voltage control flexibility is proved to be more active in machines that have double stator structure, due to its sufficient set of conductors. Nevertheless, these good qualities of double stator permanent magnet machine are usually accompanied with high mechanical complexity and often with relatively high production cost.

Similarly, (Zhao *et al.*, 2021) in [7] developed a dual stator PM machine with a view to increase its torque density, relative to the existing fault-tolerant PM machines. Although, the developed dual stator PM machine has admirable fault-tolerance ability; however, it has complicated mechanical assembly and hence, would pose major challenge during the manufacturing processes. Further, a different kind of double stator permanent magnet machine having high flux-controllability aptitude, due to the nature of its implemented field winding topology in the inner stator is proposed in [8]. The developed machine in [8] is an integration of two independent machines; this combined machine has an enhanced torque density compared to a conventional dual stator flux-switching PM machine, owing to the application of consequent pole rotor arrangement on the former. However, the proposed high flux-controllability machine could experience higher eddy current loss, owing to the structural pattern of the PMs; since, it is mounted directly on the revolving section. This shortcoming may consequently reduce the overall efficiency of such machine. Above all, the compared machines in this present study would have higher propensity for increased output power and torque, since its inner and outer stator armature windings are connected in series unlike the situation in the flux-controllable machine, where the machine's inner stator windings is replaced or short-changed with field excitation coil; though, it all depends on specific applications(s).

Furthermore, a dual stator permanent machine of different structural design is developed in [9] by analytical method, for improved flux density waveform; however, the adopted analytical technique is inferior to the implemented finite element analysis (FEA) method in this current study, owing to the higher prediction accuracy of the latter. More so, a comparative study between flux-switching permanent magnet machines presented in [10] shows that the rotor-mounted-PM (RMPPM) type of the machine could have better output torque/power advantage over its stator-mounted-PM (SMPPM) counterpart. Nevertheless, the studies proved that the SMPPM machine type has better efficiency and enhanced power factor, though with lesser field-weakening ability than its RMPPM counterpart. Moreover, it is worth noting that SMPPM machine categories usually have better thermal management than the RMPPM equivalents and thus by implication, the SMPPM machine types are characterized by strong anti-demagnetization abilities, as would be re-established later in this present study. It is important to note that the investigated machines in this present study are of the SMPPM category.

Essentially, a comprehensive performance comparison of double stator permanent magnet machines is investigated and quantitatively presented in this current study. Nevertheless, the comparisons are yet to undergo laboratory tests. The presented quantitative comparisons of the investigated machines would provide good insights and guidance about the machines' general output performances and characteristics behaviour, including its level of PM usage, flux-weakening and anti-demagnetization capabilities etc. for potential practical applications(s).

2. Machine description

The compared machines in this work are designated as: Machine 1, Machine 2 and Machine 3, respectively. The compared machines are all double stator permanent magnet machines with varying structural arrangements, having two separate excitation sources. Machine 1, Machine 2 and Machine 3 are depicted in Fig. 1, Fig. 2 and Fig. 3, respectively. Machine 1 has its magnets situated in the outer stator with corresponding armature windings on both inner and outer stators. The magnets of Machine 2 are located in its inner stator while it has armature windings on its two stator parts. Similarly, Machine 3 is equipped with magnets in its inner and outer stators, though without any winding in the inner stator section. The compared machines have similar rotor structure in form of a cup; in practice, the cup-rotor would seat upon two different bearings from both ends of the rotor that coincides with the machine's end plate/cover of the frame. Although,

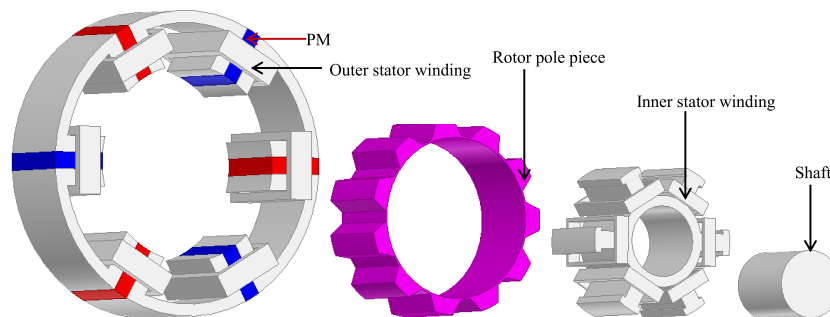


Fig. 1. Exploded view of Machine 1 [11]

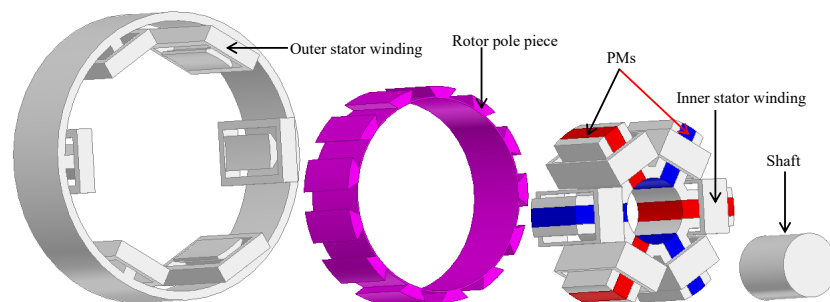


Fig. 2. Exploded view of Machine 2

the stator and rotor materials of the investigated machines are made of steel material having M330-35A grade; the stator core is stacked with laminations while the rotor is of solid core material. Practically, the mechanical stability of the rotor would be provided by a shell containing non-magnetic ribs/rods enclosed in a transparent hardened epoxy material. Note also that the rotor pieces are bridged with a steel material of 0.5 mm thickness. The shaft is made of a standard non-magnetic steel material.

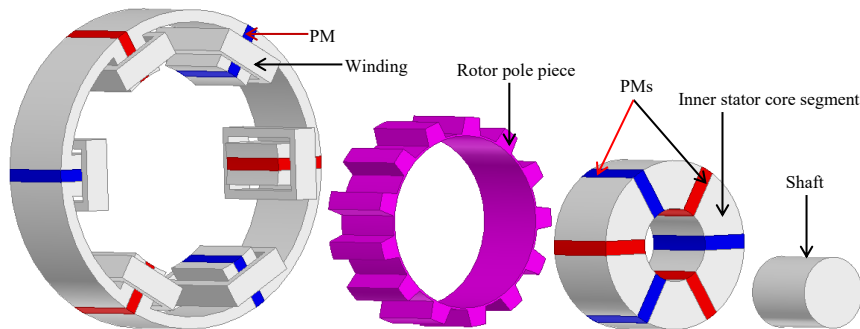


Fig. 3. Exploded view of Machine 3

The developed double stator permanent magnet machines belong to the class of flux-switching permanent magnet machines whose flux direction changes in one-half of an electric cycle, in order to yield a bipolar flux linkage and eventually produce the required induced voltage over a specified electric period. The adopted permanent magnets (PMs) in this work are placed in the stators in a radial orientation with magnets of opposite polarities placed nearby to each other in each separate stator. Also, magnets of opposite polarities are made to face directly opposite to each other, between the inner and outer stators.

More so, the investigated machines have PMs mounted in their stators in spoke-like form while utilizing the flux-focusing skill, in order to enhance the airgap flux densities of these machines and hence, improve its torque production. All the same, the major flux and torque contributions come more from the PMs than the armature windings. Note that the inner and outer stators separated by a cup rotor, are wound with concentrated armature windings and these armature windings are connected together in series for better output, though parallel winding connections are also possible. The positions of the dual stators are independent of each other, i.e. the outer stator is mounted on the motor frame while the inner stator is fixed on one side of the machine's end/cover plate. Meanwhile, the cup-shaped rotor modulates the generated magnetic fields of both permanent magnets and armature windings, for effective torque creation.

The basic elements and adopted materials of the compared machine types are itemized in Table 1. Note that, the Transient Solver Excitation Scheme of the adopted MAXWELL software is utilized in this work due to its enhanced prediction accuracy level, having specified terminals and stranded conductors with a defined number of conductors for the set of coils per phase.

Excitation of the windings would be automatically conducted by the inherent software features, considering the available slot area and the inputted coil fill factor (which is 0.6 in this case) on applying the sinusoidal three-phase currents with time-stepping technique. Although, the same

Table 1. Basic elements of the analyzed double stator machines

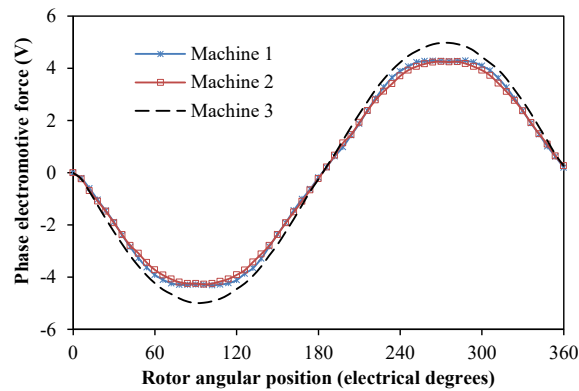
Element name	Symbol	Value	Unit		
Inner stator pole number	–	6	–		
Outer stator pole number	–	6	–		
Air-gap size	–	0.5	mm		
Active axial length	L_a	25	mm		
Machine outer diameter	–	90	mm		
PM relative permeability	μ_r	1.05	–		
Operating frequency	f	50	Hz		
Applied current amplitude	I	15	A		
Grade of magnet	–	N35SH	–		
Stator and rotor core material	–	M330-35A	–		
Coil material	–	Copper	–		
Hysteresis loss constant	k_h	0.0179	–		
Excess loss constant	k_e	0.0002	–		
Lamination width	L_w	0.5	mm		
Material conductivity	σ	2.22×10^6	(Siemens/m)		
PM remanence	–	1.2	Tesla		
Coil fill factor	–	0.6	–		
Total number of turns/phase	–	72	–		
Machine type	Machine 1	Machine 2	Machine 3	Symbol	Unit
	Value				
Rotor pole number	11	13	13	P_r	–
Phase resistance at 20°C	0.0358	0.0328	0.0493		Ohms
Number of inner stator coils/phase	2	2	–	–	–
Number of outer stator coils/phase	2	2	2	–	–
Number of inner stator turns/coil	12	12	–	–	–
Number of outer stator turns/coil	24	24	36	–	–
Rotor core volume, 3D	11 891.56	10 193.75	10 809.34	–	mm ³
Stator core volume, 3D	53 926.97	44 576.30	63 947.32	–	mm ³
PM volume, 3D	11 905.07	16 394.17	15 745.40	–	mm ³

total number of turns are allocated per phase in each of the compared machines, for fairness. However, it is worth noting that the allocation of turns per coil in each separate stator is done using the available slot areas as the benchmarks, in order to maintain same level of current density in

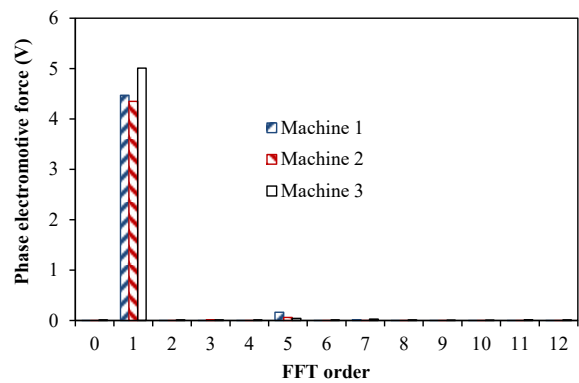
both stators; though, independently for the various machine types. Note that the coloured red and blue PMs indicate that the adjacent magnets have equal and opposite magnetization directions and values.

3. Open-circuit performance

The phase electromotive force waveforms with its corresponding harmonic spectra are shown in Fig. 4. The operating rotor speed of the compared machines at open circuit condition is 400 rpm. It is obvious that the induced electromotive force (EMF) waveforms of both Machines 1 and 2 are not completely sinusoidal, and this defect may be detrimental to effective or efficient control of such machines. Machine 3 is shown to have the highest value of induced-EMF of about 4.98 V; while Machines 1 and 2 have comparable peak EMF values of about 4.29 V and 4.26 V, respectively. More so, the resulting electromotive force values of a given machine



(a) Waveforms



(b)

Fig. 4. 2D-FEA comparison of phase electromotive force at 400 rpm: waveform (a); spectra (b)

would be a function of the applied magneto-motive force amplitudes, when operated on load conditions. Nevertheless, the manifestation of the 5th EMF harmonic order shown in Fig. 4(b) reveals that the analyzed machines would have torque ripple effect, as reported in [12]. Moreover, if the induced-EMF waveform of a given machine is not in phase with that of the operating voltage, then, there could be potential demagnetization risk in the device, as highlighted in [13]. However, the demagnetization level of the machine is majorly dependent on its phase resistance component; though, this demerit could be minimized through adequate optimization and design techniques.

Figure 5 shows the variation of fundamental voltage values with the rotational speed of the machines, obtained using fast Fourier transformation (FFT) technique. It is noticed that the generated voltage varies directly proportional to the rotor speed. Also, it is shown that Machine 3 is the most promising candidate amongst the compared machines; these voltage values would subsequently influence the overall electromagnetic torque of the machines. The small amount of induced voltage in the compared machines is mainly caused by the adverse effect of its relatively small ratio between the machines' active axial length and the overall stator diameter, as established in [14]. Low EMF output characteristics due to the adverse effect of small ratio between the machine's active stack or axial length and its outer diameter is also applicable to other permanent magnet machines, as proved in [15]. In addition to the low output voltage of the analyzed double stator flux-switching permanent magnet (DS-FSPM) machines; FSPM machines are generally associated with high flux leakages, as presented in [16] and [17].

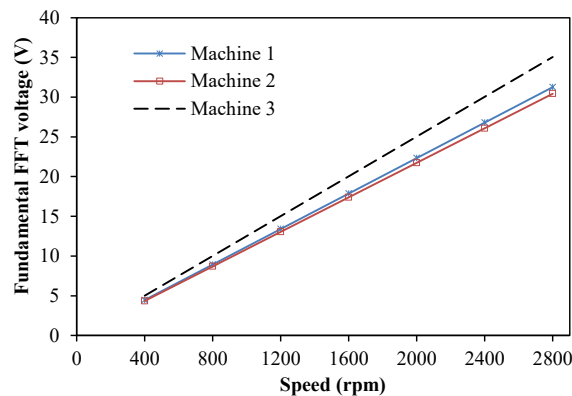


Fig. 5. Variation of fast Fourier transform (FFT) induced-EMF with speed, 2D-FEA

4. Load characteristics

As inferred from Fig. 6, the static torque difference between the predicted 2D-FEA and 3D-FEA results at 15 A from Machine 1, Machine 2 and Machine 3 is 13.4%, 19.7% and 9.10%, respectively. The results are reasonably good, considering the small total size of the machines coupled with the influence of end-windings. Note that the least discrepancy is exhibited by

Machine 3, since only one side of its two stators is equipped with windings, thus there is less end-effect in Machine 3 topology. I_A , I_B and I_C are the supplied current amplitudes in the three-phases.

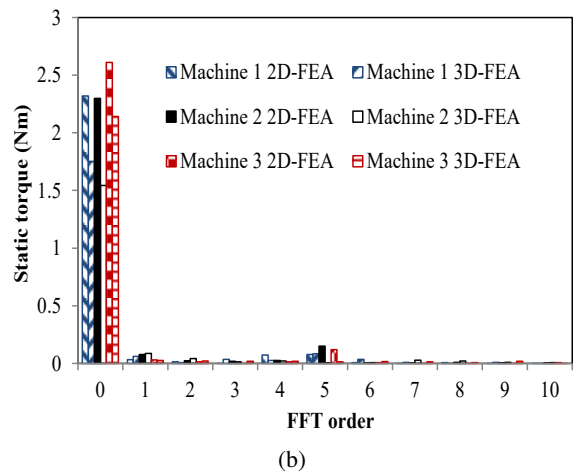
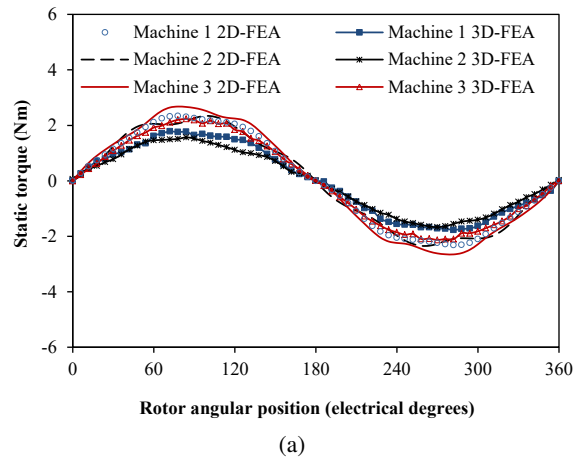


Fig. 6. Comparison of static torque at $I_A = 15$ A and $I_A = 2I_B = -2I_C$, 400 rpm: waveforms (a); spectra (b)

The applied sinusoidal three-phase AC excitation current waveform of the analyzed machines is depicted in Fig. 7, having peak current amplitude of 15 A. More so, the electromagnetic torque of the compared machines is presented in Fig. 8. The largest electromagnetic torque is obtained in Machine 3; while Machines 1 and 2 have almost similar electromagnetic torque magnitudes. Further, the predicted 2D-FEA average torque is 2.34 Nm, 2.27 Nm and 2.63 Nm, i.e. from Machine 1, Machine 2 and Machine 3, respectively with corresponding 3D-FEA values of 1.75 Nm, 1.54 Nm and 2.16 Nm, respectively. Again, Machine 3 is the most competitive candidate

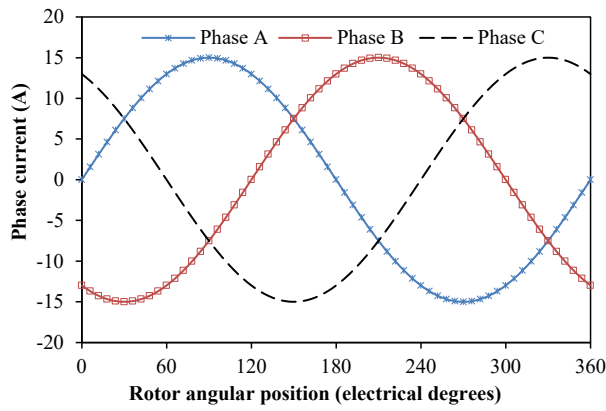
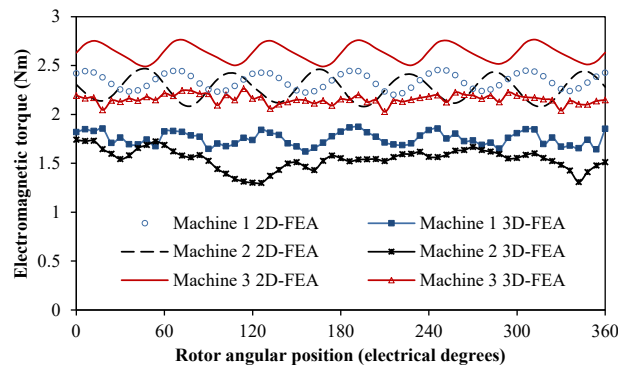
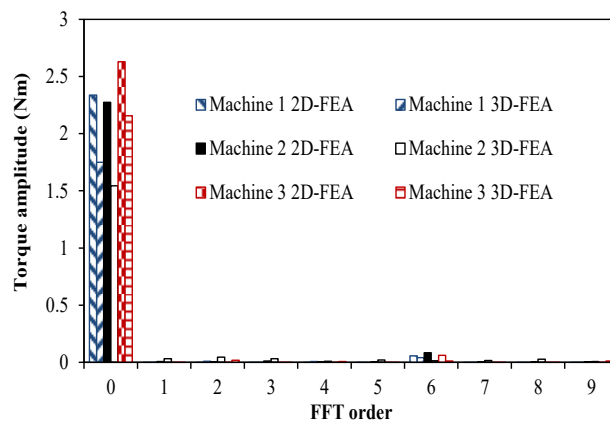


Fig. 7. Applied three-phase current waveform



(a)



(b)

Fig. 8. Comparison of output electromagnetic torque at 15 A, 400 rpm: waveforms (a); spectra (b)

amongst all. The differences between 2D-FEA and 3D-FEA torque values are mainly due to the small ratio of active axial length to machine diameter (l_{ad}) coupled to the attendant end-winding effect. The impact of active axial length to machine overall diameter proportion is emphasized to be considerably high [14] and [18] in machines that have small ratios of l_{ad} . It is important to recall that the l_{ad} ratio of the analyzed machines in this present study is 25:90, i.e. only about 0.27, which is quite little compared to what is obtainable in most other electrical machines of similar size. The electromagnetic torque (T_o) mathematical expression of the compared machines is given in (1).

$$T_o = \frac{N_{ph}}{2} P_r [\psi_{pm} I \cos(\alpha) - (L_d - L_q) I^2 \sin(\alpha) \cos(\alpha)], \quad (1)$$

where: N_{ph} is the number of phases, i.e. 3 in this present case, P_r is the rotor pole number, ψ_{pm} is the flux linkage contribution from magnets, L_d and L_q are the direct and quadrature axis inductances, α is the torque angle, and I is the supplied current amplitude [19].

Also, the analyzed machines have noticeable 6th order torque harmonics, as shown in Fig. 8(b); and that implies that the machines would have unwanted cogging torque and torque ripple elements. The estimated cogging torque and torque ripple values of the compared machines are given in Table 2. It is shown in Fig. 9, that Machine 2 would suffer more from magnetic saturation

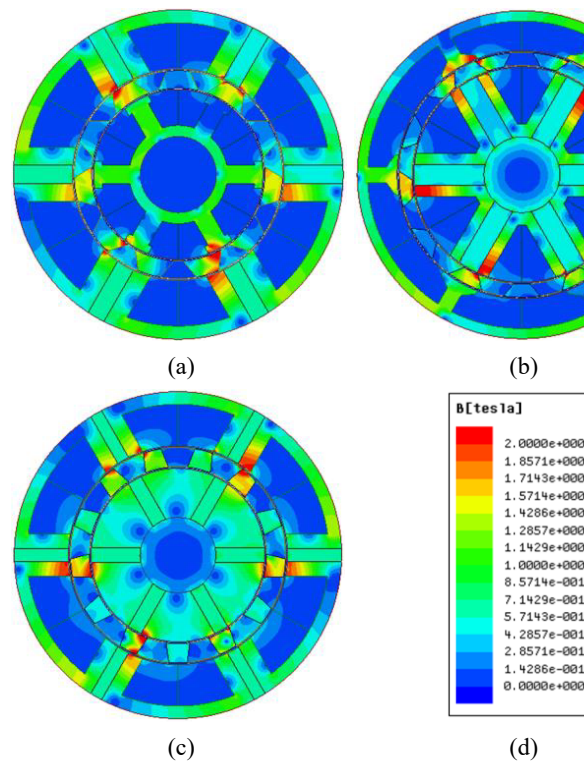


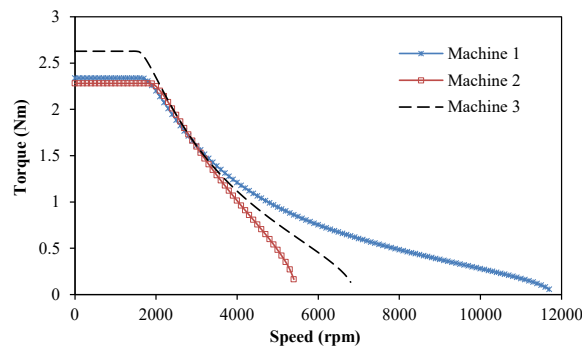
Fig. 9. 2D-FEA flux density distributions at 15 A, 400 rpm: Machine 1 (a); Machine 2 (b); Machine 3 (c); scale (d)

effects of both the PMs and the armature reaction. More so, the compared machines have higher tendency to saturate quicker in the regions closer to the machines' airgap, as can be observed from the flux density contours.

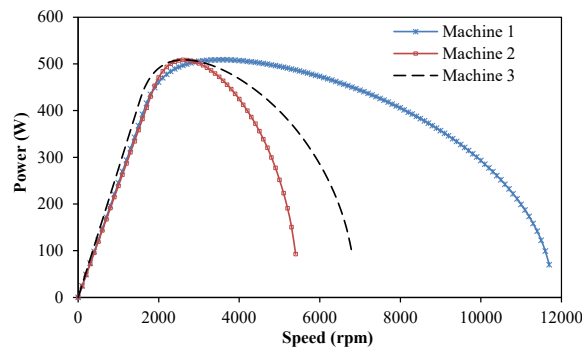
$$k_p = \frac{L_d I}{\psi_{pm}}, \quad (2)$$

where: L_d is the d -axis inductance, I is the supplied current amplitude, ψ_{pm} is the generated flux by the magnets.

Figure 10 shows the torque-speed and power-speed characteristics of the investigated machines, calculated under the maximum torque per ampere and field-weakening control techniques. It is worth mentioning that a negative direct-axis current is injected into the machine from the base speed point and beyond, i.e. in the constant power region. The implemented maximum current (I) and maximum DC voltage (V_m) limits are 15 A and 22.9 V, respectively. It is worth noting that Machine 3 has the most estimable torque-speed outline as shown in Fig. 10(a); although, the result of the flux-weakening potential provided in Table 2 shows that Machine 1 has the best flux-weakening competency, owing to the high ratio of its maximum speed (n_{max}) to base speed



(a)

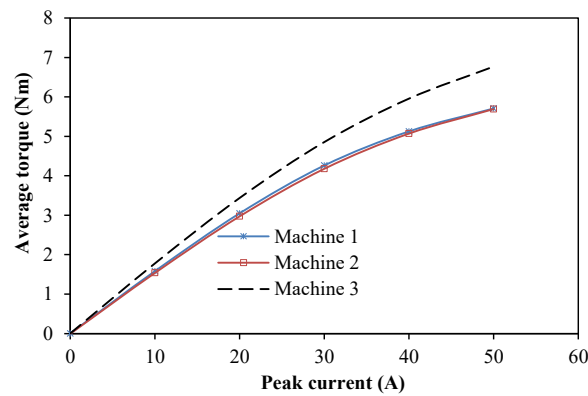


(b)

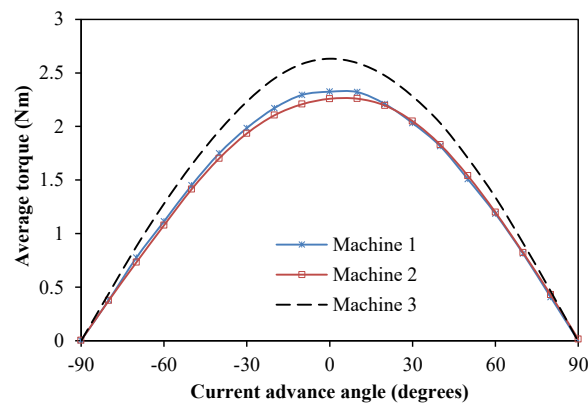
Fig. 10. Comparison of torque and power characteristics: torque versus speed (a); power versus speed (b)

(n_{base}) as well as its admirable flux-weakening factor (k_p), obtained using (2). Note also that the worst flux-weakening scenario is found in Machine 2. Thus, the enhanced flux-weakening ability of Machine 1 would give it leverage to operate over a wider speed range compared to Machines 2 and 3. Also, the analyzed machines have comparable peak power of 508.65 W, 508.68 W and 508.72 W, for Machine 1, Machine 2 and Machine 3, respectively at 3600 rpm, 2600 rpm and 2600 rpm, correspondingly.

Further, the average torque variations with both peak currents and current angles are presented in Fig. 11(a) and 11(b), operated at 400 rpm. It is observed that Machine 3 exhibits the largest overload withstand capacity amongst the compared machines. Meanwhile, Fig. 11(b) reveals that the compared machines have negligible reluctance torque with practically unity saliency ratio, and thus, would be amenable to $i_d = 0$ control scheme (i_d is the direct-axis current) [20], since its maximum average torque occurs at the zero current angle value. This assertion about the reasonably unity saliency ratio is ascertained in Table 2.



(a)



(b)

Fig. 11. Average torque comparison: torque versus current (a); torque versus current angle at 15 A (b)

Although, Machine 3 exhibits more estimable machine characteristics compared to Machine 1 and Machine 2; however, it uses relatively large volume of the permanent magnet (PM). This may increase its overall production cost; nevertheless, Machine 2 consumes the largest amount of PM material amongst the compared machines, without a commensurate overall output performance, as shown in Table 1.

The permanent magnet demagnetization characteristics of the investigated machines are displayed in Fig. 12. The demagnetization analysis is conducted at different negative direct-axis currents under flux-weakening condition. It could be observed that the PMs might experience

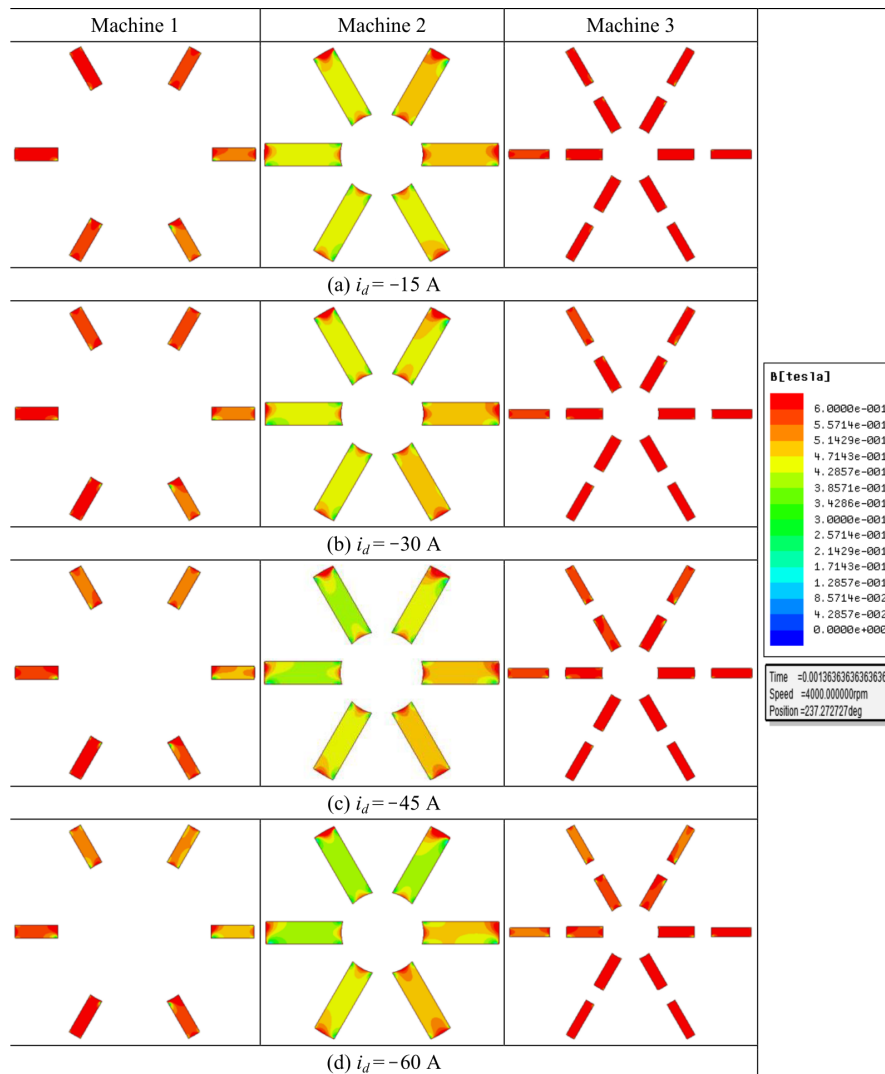


Fig. 12. Demagnetization outlines of the compared machines in flux-weakening mode at 4000 rpm, 20°C: $i_d = -15$ A (a); $i_d = -30$ A (b); $i_d = -45$ A (c); $i_d = -60$ A (d)

minor demagnetization impacts, probably at very high operating conditions; the signs of possible partial demagnetization could be seen mainly at the edges of the magnets, where there is distinct colour disparity from that of the designated topmost flux density amplitude (i.e. the PM regions that have minimum display of flux density). The tendency of demagnetization impacts would intensify at higher values of the direct-axis demagnetizing current. Moreover, Machine 3 seems to have the greatest potential against demagnetization influence, followed by Machine 1. Meanwhile, Machine 2 would most likely have the highest predisposition to be demagnetized. Note that non-linearity effect of the magnets' knee point is not applicable in this study, since the investigation is undertaken at 20°C of a given Nd-Fe-B magnet, where a straight magnetization recoil line is obtainable. More so, FSPM machines have natural ability to withstand demagnetization influence compared to other permanent machines, due to the synergy arrangement between the magnetomotive force (MMF) paths produced by both the stator currents and PM magnetic fields, as demonstrated in [21]. However, the impact of demagnetization on the contours of Fig. 12 could escalate at high operating temperature and load; because demagnetization effect is directly influenced mainly by these two factors, as could be inferred from [22] and [23].

5. Losses and efficiency

Loss estimation of electrical machines is important because both the thermal limits and efficiencies of such machines are considerably affected by its loss contents. Meanwhile, the eddy current loss in electrical systems/devices having permanent magnets, could lead to potential demagnetization of the magnets, particularly at high operating situations, as proved in [24]. Thus, loss and efficiency profiles of the compared machines are considered in this section. The core loss densities of the compared machines are displayed in Fig. 13, operated at rotor speed of 400 rpm. It is observed that the machine parts equipped with armature windings have higher loss densities than the other regions; likely due to the impact of armature reactions which would invariably increase the saturation level of such parts. Similarly, the PM eddy current loss contents of the investigated machines are compared in Fig. 14(a), at different rotor angular positions and rotational speed of 400 rpm. It is shown that Machine 3 has the least amount of PM eddy current loss; though, further PM eddy current loss reductions could be achieved in all the machines by employing magnet segmentation approach, demonstrated in [25] and [26], for a given permanent magnet machine. As mentioned earlier, PM eddy current loss in a given system could result to failure of the magnets if not minimized, especially at high working conditions of speed and load. Nevertheless, magnet segmentation generally reduces the output performance of the machine slightly and may also introduce some mechanical instability in the system [27].

Further, the core loss comparison of the investigated machines presented in Figs. 14(b) and 14(c) reveals that Machine 3 has the lowest amount of stator core loss; however, with high amount of rotor core loss. Also, the implemented non-linear magnetization and applied field (B-H) curve of the magnetic steel core material is depicted Fig. 14(d). Moreover, it is shown that Machine 3 has the largest total loss value and consequently the poorest efficiency, as depicted in Fig. 15. It is worth mentioning that the finite element predicted core loss values of a given electric machine could differ significantly from that of the fabricated prototype, owing to factors such as the adopted core-cutting patterns and the consequent lamination punching processes.

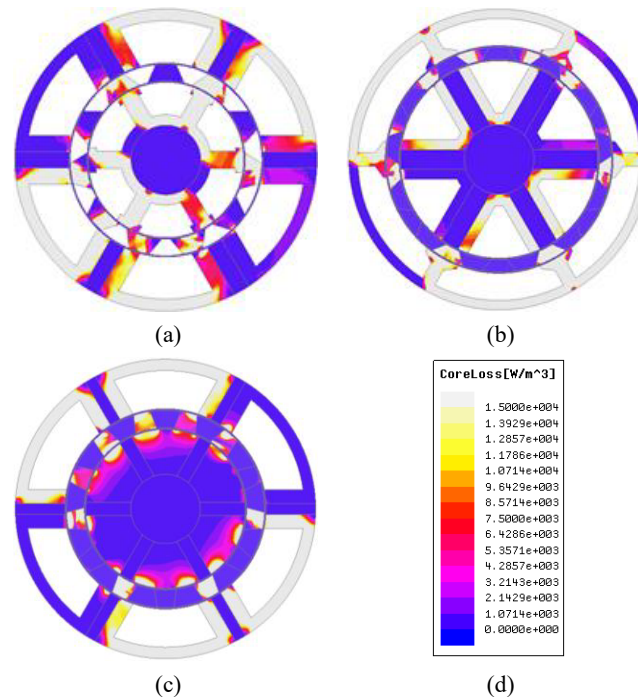


Fig. 13. Core loss density contours at 15 A, 400 rpm: Machine 1 (a); Machine 2 (b); Machine 3 (c); scale (d)

Additionally, the grades of the core materials could also influence the magnitude of core loss in a given device. Therefore, core materials with high permeability skill is often recommended for a resultant low core loss value [28], and accordingly with low relative permeability of the core sheet, as established in [29]. The predicted core loss value (W_c) per unit volume is calculated using the traditional Bertotti's loss formular given in (3). It is observed that copper losses are usually very high in high torque low speed machines, as detailed and proved in [30].

Furthermore, it is shown in Fig. 15 that the investigated machines have comparable maximum efficiencies, though Machine 2 has slight competitive efficiency advantage over others. The efficiency was calculated at a supplied current of 15 A and rotor speed of 400 rpm. The corresponding rated power at such conditions is 97.93 W, 95.24 W and 110.17 W for Machine 1, Machine 2 and Machine 3, respectively. More details about the predicted losses and the implemented material constants in this current study are provided in Table 1. Also, the estimated losses of the compared machines are enumerated in Table 2. The rotational losses in an electrical machine primarily occurs due to its bearing friction and consequently, by the windage effect. The friction loss (W_f) and windage loss (W_d) of the compared machines is predicted with the mathematical expressions given in (4) and (7), respectively.

$$W_c = \left[k_h f B_m^2 + \frac{\sigma L_w^2}{12T} \int \left(\frac{dB(t)}{dt} \right)^2 dt + \frac{k_e}{T} \int \left(\frac{dB(t)}{dt} \right)^{\frac{3}{2}} dt \right], \quad (3)$$

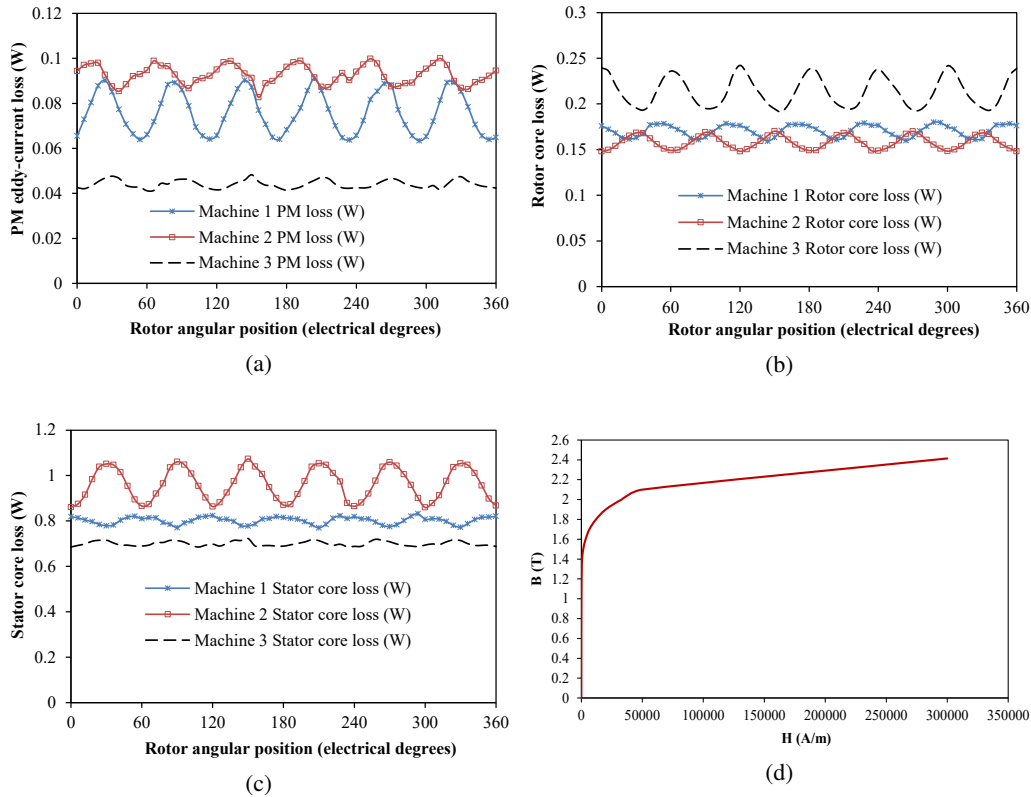


Fig. 14. Loss comparison at 400 rpm and 15 A, plus magnetization and applied field ($B - H$) curve: PM eddy current loss (a); rotor core loss (b); stator core loss (c); $B - H$ curve (d)

where: k_h and k_e , are the hysteresis and excess loss constants [31], f is the operating frequency, B_m is the maximum flux density, L_w is the lamination width, σ is material conductivity, T is the time: the integration limits are from 0 to T , and V_{core} is the core volume.

$$W_f = R_c F_c \pi \rho_a \omega_r^3 r^4 L_a, \quad (4)$$

where: R_c is the roughness constant (the value is 1.0 for a smooth surface and 2.5 for axially slotted surface), F_c is the friction constant, ρ_a is the air density, ω_r is the shaft rotational speed, r is the rotor radius, L_a is the machine's active stack length [32].

Meanwhile, the expression for Reynolds's number (N_{Re}) is given in (5). Similarly, the friction constant (F_c) is calculated using (6), while the torque constant (T_c) is estimated using (8). Generally, low speed high torque machines are usually characterized by low efficiency due to its enormous loss profile, especially at high load, as noted in literature [8]. Overall, the obtained results in Fig. 15(b) show that the investigated double stator machines have reasonably good efficiencies.

$$N_{\text{Re}} = \frac{\rho_a \omega_r D_{\text{rot}} l_g}{2\mu_{va}}, \quad (5)$$

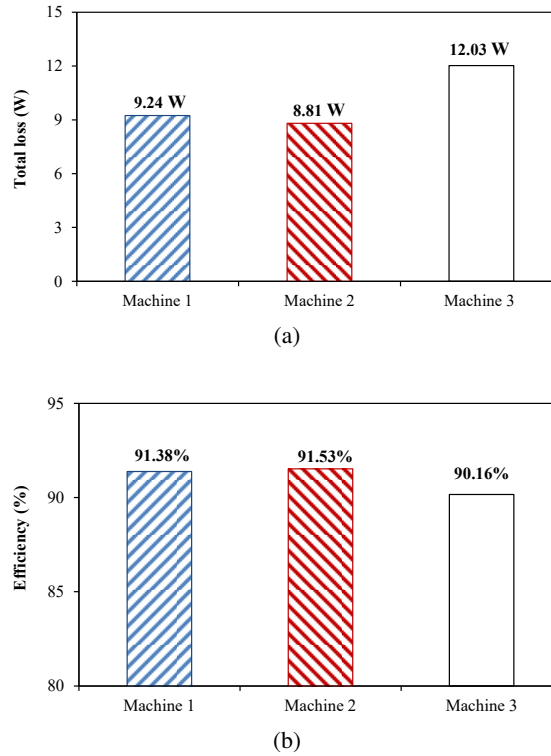


Fig. 15. Comparison of loss and efficiency, 2D-FEA at 400 rpm, 15 A: total loss (a); efficiency (b)

where l_g is the airgap length and μ_{va} is the air dynamic viscosity (18.6 μ Pa).

$$F_c = 0.515 \frac{(l_g/r)^{0.3}}{(N_{Re})^{0.5}}, \quad (6)$$

$$W_d = 0.03125 \omega_r^3 \pi T_c R_c \rho_a D_{rot}^4 L_a, \quad (7)$$

where: T_c is the torque constant, R_c is the roughness constant, ρ_a is the air density (1.184 kg/m³), D_{rot} is the rotor diameter, and L_a is the rotor active length [33].

$$T_c = 1.03 \frac{(2l_g/D_{rot})^{0.3}}{(N_{Re})^{0.5}}. \quad (8)$$

The estimated efficiency (η) of the analyzed machines is predicted using (9). Some of the analyzed machine parameters and the obtained 2D-FEA numerical result values are summarized in Table 2.

$$\eta = \frac{P_o}{P_o + W_c + W_{pm} + W_{cu} + W_f + W_d} \times 100, \quad (9)$$

where: P_o is the mechanical output power, W_c is the total core loss, W_{pm} is the permanent magnet eddy-current loss, W_{cu} is the copper loss, W_f is the friction loss, W_d is the windage loss.

Table 2. A summary of the obtained 2D-FEA numerical results

Machine topology	Machine 1	Machine 2	Machine 3	Symbol	Unit
	Value				
Peak flux linkage on no-load	9.64	7.98	9.18	–	mWb
Cogging torque	0.0718	0.1440	0.1210	–	Nm
Current density	4.45	4.07	6.12	J	A/mm ²
Torque ripple	10.78	16.85	10.48	–	%
Reluctance torque	0.0041	0.02985	0.0043	–	Nm
Average torque at rated current	2.3379	2.2738	2.6301	–	Nm
Minimum torque at rated current	2.1997	2.0841	2.4908	–	Nm
Maximum torque at rated current	2.4517	2.4673	2.7664	–	Nm
Copper loss at rated current	8.0616	7.3771	11.0925	W_{cu}	W
Friction loss at 400 rpm	0.0856	0.1419	0.096	W_f	mW
Windage loss at 400 rpm	0.0478	0.0793	0.054	W_d	mW
Total core loss at 400 rpm	0.9725	1.1202	0.7439	W_c	W
PM eddy current loss at 400 rpm	0.0759	0.0928	0.0440	W_{pm}	W
Base speed	1 700	1 900	1 600	n_{base}	rpm
Maximum speed	11 700	5 400	6 800	n_{max}	rpm
n_{max}/n_{base}	6.88	2.84	4.25	–	–
Flux-weakening factor	0.7845	0.5571	0.6746	k_p	–
d -axis inductance	0.4940	0.2892	0.4040	L_q	mH
q -axis inductance	0.4925	0.3230	0.4138	L_d	mH
Saliency ratio	0.9970	1.1166	1.0242	L_q/L_d	–

6. Conclusion

Characteristics and performance comparisons of three (3) different kinds of double stator permanent magnet machines are presented in this study using both 2D-FEA and 3D-FEA techniques. Machines 1, Machine 2 and Machine 3 are all double stator permanent magnet machines with different structural arrangements having two separate excitation sources. Machine 1 has its magnets situated in the outer stator with accompanying armature windings on both inner and outer stators. The magnets of Machine 2 are located in its inner stator while it has armature windings on its two stator parts. Similarly, Machine 3 is equipped with magnets in its inner and outer stators, though without any winding on the inner stator section.

The results show that the analyzed Machine 3 has the most competitive performance such as: the largest average torque and electromagnetic torque, enriched EMF waveform and amplitude;

albeit, with the largest total loss and least efficiency values. Also, Machine 1 has the most promising flux-weakening proficiency; hence, would possess the ability to be driven over the widest speed range amongst the compared machines. Moreover, Machine 3 seems to have the greatest potential against demagnetization influence, followed by Machine 1. Meanwhile, Machine 2 would most likely have the highest tendency to be demagnetized. The investigated machines would be suitable for direct-drive automobile uses.

Acknowledgement

I wish to thank the Commonwealth Scholarship Commission, UK, for the sponsorship to run a Ph.D. programme at the University of Sheffield, UK, during which period this research was conceived.

References

- [1] Zhu Z.Q., Li H.Y., Deodhar R., Pride A., Sasaki T., *Recent developments and comparative study of magnetically geared machines*, CES Transactions on Electrical Machines and Systems, vol. 2, no. 1, pp. 13–22 (2018), DOI: [10.23919/TEMS.2018.8326448](https://doi.org/10.23919/TEMS.2018.8326448).
- [2] Song Z., Liu C., Zhao H., *Quantitative comparison of distinct dual-stator permanent magnet vernier machines for direct-drive applications*, IEEE Transactions on Magnetics, vol. 55, no. 7, pp. 1–6 (2019), DOI: [10.1109/TMAG.2019.2914718](https://doi.org/10.1109/TMAG.2019.2914718).
- [3] Qiu H., Zhang Y., Yang C., Yi R., *Performance analysis and comparison of PMSM with concentrated winding and distributed winding*, Archives of Electrical Engineering, vol. 69, no. 2, pp. 303–317 (2020), DOI: [10.24425/ae.2020.133027](https://doi.org/10.24425/ae.2020.133027).
- [4] Baszynski M., *Torque ripple reduction in BLDC motor based on a PWM technique for open-end winding*, Archives of Electrical Engineering, vol. 70, no. 1, pp. 5–23 (2021), DOI: [10.24425/ae.2021.136049](https://doi.org/10.24425/ae.2021.136049).
- [5] Yu J., Liu C., Zhao H., *Design and multi-mode operation of double-stator toroidal-winding PM vernier machine for wind-photovoltaic hybrid generation system*, IEEE Transactions on Magnetics, vol. 55, no. 7, pp. 1–7 (2019), DOI: [10.1109/TMAG.2019.2906849](https://doi.org/10.1109/TMAG.2019.2906849).
- [6] Ma Y., Ching T.W., Fu W.N., Niu S., *Multi-objective optimization of a direct-drive dual-structure permanent magnet machine*, IEEE Transactions on Magnetics, vol. 55, no. 10, pp. 1–4 (2019), DOI: [10.1109/TMAG.2019.2922475](https://doi.org/10.1109/TMAG.2019.2922475).
- [7] Zhao Y., Huang W., Jiang W., Lin X., Wu X., *Optimal design and performance analysis of dual-stator permanent magnet fault-tolerant machine*, IEEE Transactions on Magnetics, vol. 57, no. 2, pp. 1–6 (2021), DOI: [10.1109/TMAG.2020.3026327](https://doi.org/10.1109/TMAG.2020.3026327).
- [8] Wei L., Nakamura T., *Optimization design of a dual-stator switched flux consequent pole permanent magnet machine with unequal length teeth*, IEEE Transactions on Magnetics, vol. 56, no. 2, pp. 1–5 (2020), DOI: [10.1109/TMAG.2019.2947083](https://doi.org/10.1109/TMAG.2019.2947083).
- [9] Asgari S., Mirsalim M., *A novel dual-stator radial-flux machine with diametrically magnetized cylindrical permanent magnets*, IEEE Transactions on Industrial Electronics, vol. 66, no. 5, pp. 3605–3614 (2019), DOI: [10.1109/TIE.2018.2856211](https://doi.org/10.1109/TIE.2018.2856211).
- [10] Su P., Hua W., Wu Z., Chen Z., Zhang G., Cheng M., *Comprehensive comparison of rotor permanent magnet and stator permanent magnet flux-switching machines*, IEEE Transactions on Industrial Electronics, vol. 66, no. 8, pp. 5862–5871 (2019), DOI: [10.1109/TIE.2018.2875636](https://doi.org/10.1109/TIE.2018.2875636).
- [11] Awah C.C., *A new topology of double-stator permanent magnet machine equipped with AC windings on both stators*, Archives of Electrical Engineering, vol. 71, no. 2, pp. 1–14 (2022), DOI: [10.24425/ae.2022.140711](https://doi.org/10.24425/ae.2022.140711).

- [12] Li J., Wang K., Zhang H., *Flux-focusing permanent magnet machines with modular consequent-pole rotor*, IEEE Transactions on Industrial Electronics, vol. 67, no. 5, pp. 3374–3385 (2020), DOI: [10.1109/TIE.2019.2922922](https://doi.org/10.1109/TIE.2019.2922922).
- [13] Zawilak T., *Influence of rotor's cage resistance on demagnetization process in the line start permanent magnet synchronous motor*, Archives of Electrical Engineering, vol. 69, no. 2, pp. 249–258 (2020), DOI: [10.24425/aee.2020.133023](https://doi.org/10.24425/aee.2020.133023).
- [14] Zhu Z.Q., Chen J.T., Pang Y., Howe D., Iwasaki S., Deodhar R., *Analysis of a novel multi-tooth flux-switching PM brushless AC machine for high torque direct-drive applications*, IEEE Transactions on Magnetics, vol. 44, no. 11, pp. 4313–4316 (2008), DOI: [10.1109/TMAG.2008.2001525](https://doi.org/10.1109/TMAG.2008.2001525).
- [15] Vahaj A.A., Rahideh A., Lubin T., *General analytical magnetic model for partitioned-stator flux-reversal machines with four types of magnetization patterns*, IEEE Transactions on Magnetics, vol. 55, no. 11, pp. 1–21 (2019), DOI: [10.1109/TMAG.2019.2929477](https://doi.org/10.1109/TMAG.2019.2929477).
- [16] Chen J.T., Zhu Z.Q., *Influence of the rotor pole number on optimal parameters in flux-switching PM brushless AC machines by the lumped-parameter magnetic circuit model*, IEEE Transactions on Industry Applications, vol. 46, no. 4, pp. 1381–1388 (2010), DOI: [10.1109/TIA.2010.2049720](https://doi.org/10.1109/TIA.2010.2049720).
- [17] Fei W., Luk P.C.K., Shen J.X., Wang Y., Jin M., *A novel permanent-magnet flux switching machine with an outer-rotor configuration for in-wheel light traction applications*, IEEE Transactions on Industry Applications, vol. 48, no. 5, pp. 1496–1506 (2012), DOI: [10.1109/TIA.2012.2210009](https://doi.org/10.1109/TIA.2012.2210009).
- [18] Raminosoa T., El-Refaie A.M., Pan D., Huh K.K., Alexander J.P., Grace K., Grubic S., Galioto S., Reddy P.B., Shen X., *Reduced rare-earth flux-switching machines for traction applications*, IEEE Transactions on Industry Applications, vol. 51, no. 4, pp. 2959–2971 (2015), DOI: [10.1109/TIA.2015.2397173](https://doi.org/10.1109/TIA.2015.2397173).
- [19] Yu D., Huang X., Zhang X., Zhang J., Lu Q., Fang Y., *Optimal design of outer rotor interior permanent magnet synchronous machine with hybrid permanent magnet*, IEEE Transactions on Applied Superconductivity, vol. 29, no. 2, pp. 1–5 (2019), DOI: [10.1109/TASC.2019.2895260](https://doi.org/10.1109/TASC.2019.2895260).
- [20] Shi J.T., Zhu Z.Q., Wu D., Liu X., *Comparative study of novel synchronous machines having permanent magnets in stator poles*, 2014 International Conference on Electrical Machines (ICEM), Berlin, Germany, pp. 429–435 (2014), DOI: [10.1109/ICELMACH.2014.6960216](https://doi.org/10.1109/ICELMACH.2014.6960216).
- [21] McFarland J.D., Jahns T.M., El-Refaie A.M., *Demagnetization performance characteristics of flux switching permanent magnet machines*, IEEE International Conference on Electrical Machines (ICEM), Berlin, Germany, pp. 2001–2007 (2014), DOI: [10.1109/ICELMACH.2014.6960459](https://doi.org/10.1109/ICELMACH.2014.6960459).
- [22] Baranski M., Szelag W., Lyskawinski W., *Analysis of the partial demagnetization process of magnets in a line start permanent magnet synchronous motor*, Energies, vol. 13, no. 21, pp. 5562 (2020), DOI: [10.3390/en13215562](https://doi.org/10.3390/en13215562).
- [23] Lee S.G., Kim K.S., Lee J., Kim W.H., *A novel methodology for the demagnetization analysis of surface permanent magnet synchronous motors*, IEEE Transactions on Magnetics, vol. 52, no. 3, pp. 1–4 (2016), DOI: [10.1109/TMAG.2015.2490203](https://doi.org/10.1109/TMAG.2015.2490203).
- [24] Qiu H., Zhang S., *Rotor optimization of axial-radial flux type synchronous machine based on magnetic flux leakage*, Archives of Electrical Engineering, vol. 70, no. 3, pp. 551–566 (2021), DOI: [10.24425/aee.2021.137573](https://doi.org/10.24425/aee.2021.137573).
- [25] Hu Y., Zhu S., Liu C., *Magnet eddy-current loss analysis of interior PM machines for electric vehicle application*, IEEE Transactions on Magnetics, vol. 53, no. 11, pp. 1–4 (2017), DOI: [10.1109/TMAG.2017.2700850](https://doi.org/10.1109/TMAG.2017.2700850).
- [26] Młot A., Kowol M., Kołodziej J., Lechowicz A., Skrobotowicz P., *Analysis of IPM motor parameters in an 80-kW traction motor*, Archives of Electrical Engineering, vol. 69, no. 2, pp. 467–481 (2020), DOI: [10.24425/aee.2020.133038](https://doi.org/10.24425/aee.2020.133038).

- [27] Wang Y., Ma J., Liu C., Lei G., Guo Y., Zhu J., *Reduction of magnet eddy current loss in PMSM by using partial magnet segment method*, IEEE Transactions on Magnetics, vol. 55, no. 7, pp. 1–5 (2019), DOI: [10.1109/TMAG.2019.2895887](https://doi.org/10.1109/TMAG.2019.2895887).
- [28] Boubaker N., Matt D., Enrici P., Nierlich F., Durand G., *Measurements of iron loss in PMSM stator cores based on CoFe and SiFe lamination sheets and stemmed from different manufacturing processes*, IEEE Transactions on Magnetics, vol. 55, no. 1, pp. 1–9 (2019), DOI: [10.1109/TMAG.2018.2877995](https://doi.org/10.1109/TMAG.2018.2877995).
- [29] Djelloul-Khedda Z., Boughrara K., Dubas F., Kechroud A., Tikellaline A., *Analytical prediction of iron-core losses in flux-modulated permanent-magnet synchronous machines*, IEEE Transactions on Magnetics, vol. 55, no. 1, pp. 1–12 (2019), DOI: [10.1109/TMAG.2018.2877164](https://doi.org/10.1109/TMAG.2018.2877164).
- [30] Zhang J., Zhang B., Feng G., Gan B., *Design and analysis of a low-speed and high-torque dual-stator permanent magnet motor with inner enhanced torque*, IEEE Access, vol. 6, pp. 1–12 (2020), DOI: [10.1109/ACCESS.2020.3028425](https://doi.org/10.1109/ACCESS.2020.3028425).
- [31] Thomas A.S., Zhu Z.Q., Li G.J., *Thermal modelling of switched flux permanent magnet machines*, in IEEE International Conference on Electrical Machines (ICEM), Berlin, Germany, pp. 2212–2217 (2014), DOI: [10.1109/ICELMACH.2014.6960491](https://doi.org/10.1109/ICELMACH.2014.6960491).
- [32] Huang Z., Fang J., Liu X., Han B., *Loss calculation and thermal analysis of rotors supported by active magnetic bearings for high-speed permanent-magnet electrical machines*, IEEE Transactions on Industrial Electronics, vol. 63, no. 4, pp. 2027–2035 (2016), DOI: [10.1109/TIE.2015.2500188](https://doi.org/10.1109/TIE.2015.2500188).
- [33] Dutta R., Chong L., Rahman F.M., *Analysis and experimental verification of losses in a concentrated wound interior permanent magnet machine*, Progress in Electromagnetics Research B, vol. 48, no. 3, pp. 221–248 (2013), DOI: [10.2528/PIERB12110715](https://doi.org/10.2528/PIERB12110715).